Current Applied Physics 15 (2015) 1143–1147

Contents lists available at ScienceDirect

Current Applied Physics

journal homepage: www.elsevier.com/locate/cap

Potentiostatic and galvanostatic electrodeposition of manganese oxide for supercapacitor application: A comparison study

Gomaa A.M. Ali [a, b], Mashitah M. Yusoff [a], Yun Hau Ng [c], Hong Ngee Lim [d], Kwok Feng Chong [a, *]

[a] Faculty of Industrial Sciences & Technology, Universiti Malaysia Pahang, 26300 Kuantan, Malaysia
[b] Chemistry Department, Faculty of Science, Al–Azhar University, Assiut, 71524, Egypt
[c] Particles and Catalysis Research Group, School of Chemical Engineering, The University of New South Wales, Sydney NSW 2052, Australia
[d] Department of Chemistry, Faculty of Science, Universiti Putra Malaysia, 43400 UPM Serdang, Selangor, Malaysia

ARTICLE INFO

Article history:
Received 5 February 2015
Received in revised form
18 May 2015
Accepted 25 June 2015
Available online 30 June 2015

Keywords:
Potentiostatic
Galvanostatic
Electrodeposition
Supercapacitors
Manganese oxide

ABSTRACT

The structural and electrochemical properties of manganese oxide (MnO_2) electrodeposited by potentiostatic and galvanostatic conditions are studied. X–ray diffraction analyses confirm identical MnO_2 phase (ramsdellite) are deposited under potentiostatic and galvanostatic conditions. Under comparable current density during electrodeposition, MnO_2 deposited by galvanostatic condition shows smaller crystallite size, less compact layered structure, higher surface area and wider band gap, in comparison to the potentiostatic deposition. The MnO_2 morphology difference under different electrodeposition conditions contributes to different capacitive behaviors. The lower compactness of MnO_2 deposited galvanostatically renders facile ions diffusion, leading to higher specific capacitance with low equivalent series resistance. The findings suggest galvanostatic electrodeposition is suitable to produce MnO_2 nanostructure for supercapacitor application.

1. Introduction

In recent years, MnO_2 is attracting attention for supercapacitor application, mainly due to the high abundancy of manganese [1] that contributes to low material cost as compared to the expensive ruthenium metal. Pang et al. reported high specific capacitance (700 F g^{-1}) for MnO_2 thin films in year 2000 and their findings sparked strong interest among energy research community for its application in supercapacitor electrode [2,3]. Such high capacitance value is attributed to the ions insertion/desertion within MnO_2 structure and it depends crucially on the particle size, surface area and porosity. Since then, in achieving optimized condition for the aforementioned properties, MnO_2 with different morphologies were developed, such as nanoflakes [4], nanorods [5], nanowires [6], nanopetals [7] and nanosheets [8]. In this context, the synthesis route plays a vital role in determining its morphology. The most common synthesis route for MnO_2 is chemical coprecipitation method [9,10] that involves dissolved Mn^{4+} precursor. However, the instability of Mn^{4+} precursor in the aqueous solution as well as the contact resistance between synthesized MnO_2 and current collectors hinders its common usage in electrochemical applications [11,12]. Apart from chemical coprecipitation method, electrochemical deposition was proven to be an effective method to prepare MnO_2 nanostructures [5,13,14]. There are two approaches for electrochemical deposition of MnO_2, namely anodic oxidation and cathodic reduction. Cationic Mn^{2+} precursor is commonly used in anodic oxidation while anionic MnO_4^- (Mn^{7+}) is used in cathodic reduction. In comparison, cathodic reduction offers more versatility as various metals could be co–deposited during the deposition process and the oxidation of the metallic substrate during anodic deposition could also be avoided [6,15,16]. The cathodic reduction of MnO_4^- in neutral aqueous solutions can be represented by the following reaction [17]:

$$MnO_4^- + 2H_2O + 3e^- \rightarrow MnO_2 + 4OH^- \quad (1)$$

The kinetic pathway of reducing Mn^{7+} to Mn^{4+} is an important factor in determining MnO_2 microstructure and it could be manipulated by potential and current during electrodeposition process [6,7,17]. In this context, galvanostatic and potentiostatic

* Corresponding author.
E-mail address: ckfeng@ump.edu.my (K.F. Chong).

http://dx.doi.org/10.1016/j.cap.2015.06.022
1567-1739/

techniques are widely employed to electrochemically produce MnO_2 nanostructures [6,11,13,18]. Suhasini reported the comparison study between MnO_2 films electrodeposited by potentiostatic and galvanostatic techniques, and demonstrated the galvanostatic technique could produce MnO_2 film with higher specific capacitance [19]. However, the reported study only referred to the anodic deposition of MnO_2 and there are limited studies report on the cathodic deposition of MnO_2. Herein, we report the comparative findings on the structural and electrochemical properties of MnO_2 deposited cathodically under potentiostatic and galvanostatic conditions.

2. Experimental section

MnO_2 was electrodeposited cathodically from 0.5 M $KMnO_4$ solution by potentiostatic [denoted as MnO_2(PS) hereafter] and galvanostatic [denoted as MnO_2(GS) hereafter] conditions by applying 10 V and 0.165 A cm^{-2} for 30 min at room temperature, respectively. The stainless steel substrate (1×2 cm^{-2}) was first etched in hydrochloric acid (0.1 M) and in acetone for 1 h, then washed and dried. Two pre–treated stainless steel plates were used as the electrodes. The distance between two electrodes was kept constant at 20 mm throughout the electrodeposition process. For both electrodeposition techniques, black films were obtained on the cathode and the mass was recorded after drying.

Phase identification of the films was carried out using a PHILLIPS PW1700 diffractometer equipped with an automatic divergent slit. Diffraction patterns were obtained using Cu–K_α radiation ($\lambda = 0.15418$ nm) and a graphite monochromator in the 2θ range from 5° to 80°. Sample morphology was investigated using a JEOL JSM–7800F field emission scanning electron microscope. The surface area of the samples were measured by NOVA 3200 surface area analyzer. The optical absorption spectra were measured at the wavelength range from 200 to 900 nm at room temperature using a THERMO SCIENTIFIC UV–Vis spectrophotometer. The electrochemical measurements were conducted in 1 M Na_2SO_4 with three–electrode system consisting MnO_2 coated stainless steel plate as working electrode, Ag/AgCl as reference electrode and Pt wire as counter electrode. Cyclic voltammetry (CV) tests and galvanostatic charge–discharge tests were conducted in the potential range between 0 and 1 V. Impedance data were collected from 100 kHz to 0.01 Hz, at open circuit potential with an AC amplitude signal of 10 mV. All electrochemical data were collected using AUTOLAB PGSTAT M101 potentiostat/galvanostat equipped with frequency response analyzer.

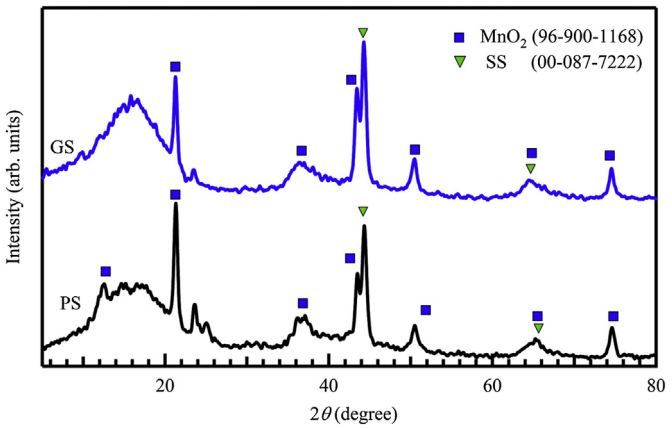

Fig. 1. XRD spectra for MnO_2(PS) and MnO_2(GS).

3. Results and discussion

Fig. 1 shows the XRD patterns of MnO_2(PS) and MnO_2(GS). Both XRD patterns confirm the black films on the stainless steel electrodes as the ramsdellite phase MnO_2 (ICCD 96 900 1168). For both XRD patterns, two XRD peaks at 44.5° and 65.8° could be attributed to the stainless steel (ICCD 00 087 7222). Crystallite size calculation by the Scherrer formula shows that the MnO_2(PS) has bigger crystallite size (23 nm) as compared to that obtained on MnO_2(GS) (18 nm). The crystallite size of MnO_2 is known to affect the ions (de) intercalation rate and therefore regulating the performance of a supercapacitor [20].

The sample morphology was investigated by FESEM and the representative images are shown in Fig. 2. Both electrodeposition conditions produce similar layered structure of MnO_2 that only differs in the nanosheets compactness. MnO_2(GS) shows lower nanosheets compactness and the nanosheets are greatly separated from each other, in comparison to the MnO_2(PS). The difference in the nanosheets compactness and morphology under different deposition conditions could be explained from the potential response (left y axis for galvanostatic) and current response (right y axis for potentiostatic) during electrodeposition process (Fig. 3). In this study, 10 V was carefully selected for the potentiostatic deposition as it generated current density in the range that was comparable to the current density applied (0.165 A cm^{-2}) in the galvanostatic deposition. The total charge passing through the electrode was calculated for both deposition conditions and they show almost identical values (293C cm^{-2} for potentiostatic; 297 C cm^{-2} for galvanostatic).

Since total consumed charge values are almost identical for both deposition processes, the difference in MnO_2 morphology could be attributed to the potential difference during electrodeposition process. For galvanostatic deposition for MnO_2(GS), it could be observed that the potential gradually decreases with time, due to the enhanced friction effect resulting from MnO_2 formation on the cathode and the interaction of ions moving in cathodic direction with the ions electromigrating in anodic direction. The potential drop decreases the diffusion rate of MnO_4^- to the cathode surface and allows lower deposition rate, thus producing MnO_2(GS) layered structure with less compact nanosheets, as shown in the FESEM image. For potentiostatic deposition for MnO_2(PS), the potential is maintained throughout the deposition process and MnO_2 structure is formed rapidly, producing layered structure with compact nanosheets. For both deposition techniques, H_2 evolution occurs and pushes the Mn species to the vacant areas of the substrate which is free from the H_2 bubbles, leading to the formation of layered structure. Similar findings are obtained elsewhere for MnO_2 and other nanomaterials [21,22].

Fig. 4 shows the N_2 adsorption–desorption isotherms of MnO_2(GS) and MnO_2(PS), with the pore size distribution as inset. The specific surface areas are found to be 63.5 and 36.6 m^2 g^{-1} for MnO_2(GS) and MnO_2(PS), respectively. Pore size distribution curves show the pore size ranges from 2 to 70 nm (two narrow peaks around 3 and 20 nm) and from 2 to 20 nm for MnO_2(GS) and MnO_2(PS), respectively. The lower nanosheets compactness of MnO_2(GS) contributes to higher surface area and wider range of mesoporousity. The mesopores play an important role in enhancing the adsorption of ions during the electrochemical measurements.

The crystallite size and morphology affect the electronic and electrochemical properties of a nanostructure. The electronic properties of MnO_2(PS) and MnO_2(GS) were investigated by band gap studies. MnO_2 exhibits broad absorption band at ca. 400 nm, which is the characteristic of the excitation from O_{2p} to Mn_{3d} [23]. The absorption band gap (E_g) was obtained from the following equation [24]: